Applied Physics Letters

Observation of carrier concentration dependent spintronic terahertz emission from *n*-GaN/NiFe heterostructures

Cite as: Appl. Phys. Lett. **117**, 093502 (2020); https://doi.org/10.1063/5.0011009
Submitted: 16 April 2020 . Accepted: 16 July 2020 . Published Online: 31 August 2020

Eric Vetter, Melike Biliroglu, Dovletgeldi Seyitliyev, Pramod Reddy, Ronny Kirste, Zlatko Sitar, Ramón Collazo, Kenan Gundogdu, and Dali Sun

COLLECTIONS

F This paper was selected as Featured

View Online

Export Citation

CrossMark

© 2020 Author(s).

Applied Physics Letters ARTICLE scitation.org/journal/apl

Observation of carrier concentration dependent spintronic terahertz emission from *n*-GaN/NiFe heterostructures

Cite as: Appl. Phys. Lett. **117**, 093502 (2020); doi: 10.1063/5.0011009
Submitted: 16 April 2020 · Accepted: 16 July 2020 ·
Published Online: 31 August 2020

Eric Vetter,[1,2] Melike Biliroglu,[1] Dovletgeldi Seyitliyev,[1] Pramod Reddy,[3] Ronny Kirste,[3] Zlatko Sitar,[2] Ramón Collazo,[2] Kenan Gundogdu,[1,4,a)] and Dali Sun[1,4,a)]

AFFILIATIONS

[1]Department of Physics, North Carolina State University, Raleigh, North Carolina 27695, USA
[2]Department of Materials Science and Engineering, North Carolina State University, Raleigh, North Carolina 27695, USA
[3]Adroit Materials, Inc., 2054 Kildaire Farm Rd., Cary, North Carolina 27518, USA
[4]Organic and Carbon Electronics Lab (ORaCEL), North Carolina State University, Raleigh, North Carolina 27695, USA

[a)]Authors to whom correspondence should be addressed: kgundog@ncsu.edu and dsun4@ncsu.edu

ABSTRACT

The development of terahertz (THz) spintronics has created a paradigm shift in the generation of THz radiation through the combination of ultrafast magnetism and spin-based electronics. However, research in this area has primarily focused on all-metallic devices comprising a ferromagnetic thin film adjacent to a non-magnetic heavy metal. Here, we report the experimental observation of spintronic THz emission from an n-doped wide bandgap semiconductor, *n*-GaN. We found that the amplitude of THz emission strongly depends on the carrier concentration of the semiconductor layer, which could be attributed to the tunable Rashba state occurring at the *n*-GaN/ferromagnet interface. Our work offers exciting prospects for pursuing wide bandgap semiconductor-based spintronic THz devices and demonstrating their intriguing spin Hall physics at the ultrafast timescale.

Published under license by AIP Publishing. https://doi.org/10.1063/5.0011009

The generation and detection of terahertz (THz) radiation is of immense technological importance for a variety of current and future applications such as non-destructive examination,[1–5] wireless communication,[6–8] and ultrafast computing.[9,10] Recently, a different mechanism for the generation of THz radiation via ultrafast spintronics has opened the door to search for emergent material classes and devices and offered the possibility for THz device functionalities.[11–13] These devices are all-metallic in nature and comprise a ferromagnetic thin film adjacent to a non-magnetic heavy metal with strong spin–orbit coupling (e.g., $Ni_{81}Fe_{19}$/Pt).[13–16] Here, the principle of operation is based on ultrafast demagnetization of the ferromagnetic thin film in response to an incident, femtosecond laser pulse, followed by conversion of the resulting superdiffusive spin current into a transient THz electric field via spin-to-charge conversion processes [e.g., inverse spin Hall effect (ISHE)[17]] in the adjacent heavy metal. These spintronic THz emitters may outperform most semiconductor-based THz emitters in terms of ultrabroadband THz emission up to 20 THz (Ref. 18) comparably cheap and facile production, and the ability to be manufactured on flexible substrates.[14] Their spintronic nature also allows for additional functional controls, such as phase reversal of the emitted THz waveform by reversal of the polarity of an applied magnetic field.[12] However, these metallic-based devices lack certain desirable attributes of their semiconductor counterparts such as the ability to be electronically doped or electrically gated, providing a barrier to further device optimization and functionalities.

Besides the metallic materials systems, spintronic THz generation has also been recently reported in a two-dimensional semiconductor, MoS_2,[19] showing the ability to convert a "giant" ultrafast spin current injected across the metal/semiconductor interface owing to a sizable bandgap in the semiconductor. Upon femtosecond laser excitation, only the spin-polarized electrons with excitation energy higher than the semiconductor's conduction band minimum can be transmitted through the metal/semiconductor interface, resulting in a highly spin-polarized current in the semiconducting layer.[19] It is, thus, anticipated that a high bandgap semiconductor forming a larger Schottky barrier may act as a more efficient spin filter by which a higher intensity spintronic THz emission can be generated.[19]

Published under license by AIP Publishing

Gallium nitride (GaN) is a well-known wide bandgap (3.4 eV) semiconductor lauded for its remarkable optoelectronic properties that make it an ideal candidate for high-power and high-frequency devices and applications.[20,21] Intriguingly, due to its non-centrosymmetric, polar wurtzite crystal structure, it has also been shown to possess a spin-split electronic band structure due to the bulk inversion asymmetry of the crystal lattice, i.e., a Rashba state [$\alpha_R = (4.5 \pm 1)$ meV A (Ref. 22)], allowing for large spin-to-charge conversion efficiencies for spintronic applications.[23] Taken together, these remarkable properties make bulk GaN a prime material candidate for use in ultrafast THz spintronics. The convergence of spintronic THz generation and these robust wide bandgap semiconductor materials would result in next generation of spintronic THz emitters with advanced semiconductor-based capabilities.

Here, we present a wide bandgap semiconductor-based spintronic THz emitter comprising a ferromagnetic thin film ($Ni_{81}Fe_{19}$) interfaced with an n-doped, wide bandgap semiconductor (*n*-GaN). We conduct THz time-domain spectroscopic measurements of the emitted THz electric fields as a function of carrier concentration in the semiconductor material. We found that the emitted THz field amplitude is strongly dependent on the carrier concentration in the *n*-GaN layer, pointing to an exciting convergence of wide bandgap semiconductors and ultrafast spintronics for both fundamental spintronic physics and THz device functionalities.

All Ga-polar *n*-GaN samples studied here were grown on sapphire substrates in a vertical, cold-walled, RF-heated, low pressure metalorganic chemical vapor deposition (MOCVD) reactor.[24] Systematic variation of the carrier concentration was achieved through doping with either Si or Ge. The doped carrier concentration and electron mobility in the *n*-GaN layers were determined through room temperature Hall effect measurements in a van der Pauw configuration.[24] The morphology of the prepared n-GaN surface is characterized by Atomic Force Microscopy (AFM). A top $Ni_{81}Fe_{19}$ (NiFe) layer is deposited using electron beam evaporation onto a 10×10 mm area of the *n*-GaN film, with a thickness of 5 nm. THz experiments are carried out using the output of a 1 kHz repetition rate Ti:sapphire amplifier (Quantronix Integra-C). The central wavelength is 800 nm and pulse duration is 120 fs.[18] The E_y and E_x components of THz radiation were recorded using a pair of wire-grid polarizers. A 300 mT in-plane external magnetic field is applied to the THz samples, which is sufficient to magnetize the NiFe layer along the in-plane direction during the measurements (Fig. 1). All measurements are taken at room temperature.

Figure 1(a) shows a schematic illustration of the sample devices and THz emission process, with a representative AFM image of the prepared *n*-GaN film prior to deposition of the NiFe layer shown in the top left inset. Here, a femtosecond laser pulse is used to excite the ferromagnetic NiFe layer, whose magnetization direction is controlled by an external permanent magnet, resulting in ultrafast demagnetization.[25] Subsequently, a high energy, superdiffusive spin current is generated[26–28] and injected across the interface into the adjacent non-magnetic *n*-GaN film where it is converted into a transient THz electric field via a spin-to-charge conversion processes.[12] Since *n*-GaN has a non-centrosymmetric wurtzite structure and the presence of Rashba states in this system has been well documented,[29,30] it is expected that the spin-to-charge conversion process here is dominated by the Inverse Rashba Edelstein Effect (IREE) rather than the Inverse Spin Hall Effect (ISHE) given the weak spin–orbit coupling

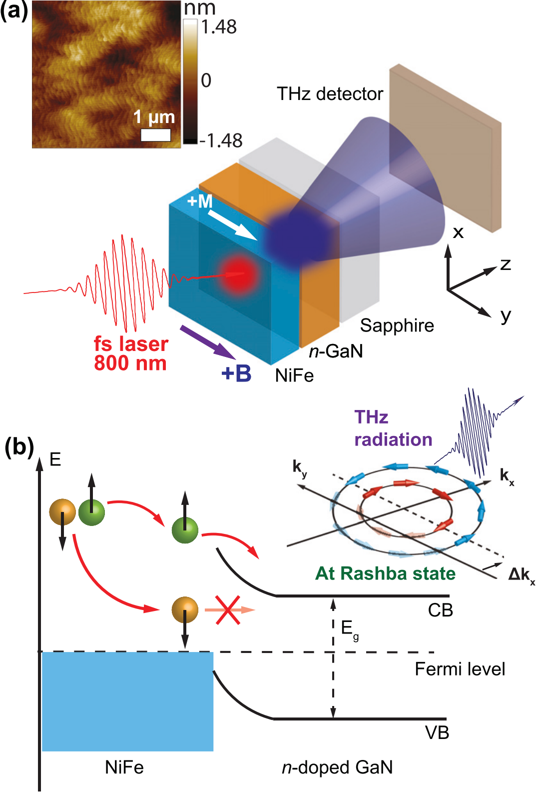

FIG. 1. (a) A sketch of spintronic THz radiation generated from a doped wide bandgap semiconductor, *n*-GaN, via an efficient spin-to-charge conversion process upon excitation from ultrafast laser pulses. The top left inset shows a representative AFM image of a fabricated *n*-GaN film, showing a smooth and uniform morphology with RMS less than 1.48 nm. (b) Schematic of spin injection from NiFe into the wide bandgap *n*-GaN semiconductor, where majority spin polarized electrons are able to enter the semiconductor's conduction band while minority spin polarized electrons rapidly decay and are blocked from entering by the high Schottky barrier formed at the NiFe/n-doped GaN interface.

provided by light elements comprising the material. The emitted THz waveform is then electro-optically detected using a 1 mm thick [110] ZnTe crystal. Figure 1(b) schematically depicts the spin injection process whereby spin-polarized minority carriers decay rapidly in energy and are filtered by the high Schottky barrier formed at the NiFe/*n*-GaN interface, while majority spin carriers are able to enter the conduction band of the semiconductor.[19,31]

In Figs. 2 and 3, a series of control experiments has been performed in order to confirm the spintronic origin of the emitted THz pulse. A typical spintronic-THz emission waveform is shown in Fig. 2(a) under both positive and negative applied magnetic fields, demonstrating the spintronic nature of the emission process in which the phase of the THz waveform is inverted with a reversal of the magnetic field polarity. The laser power dependence of the peak THz intensity is depicted in Fig. 2(b), showing that the THz electric field scales nearly linearly at low laser pump fluences. A pronounced super-linear power dependence indicates a possible high-order effect caused by multi-excitation mechanism.[32] Figure 2(c) plots the peak THz intensity as a function of linear polarization angle (θ_p) of the incident

Published under license by AIP Publishing

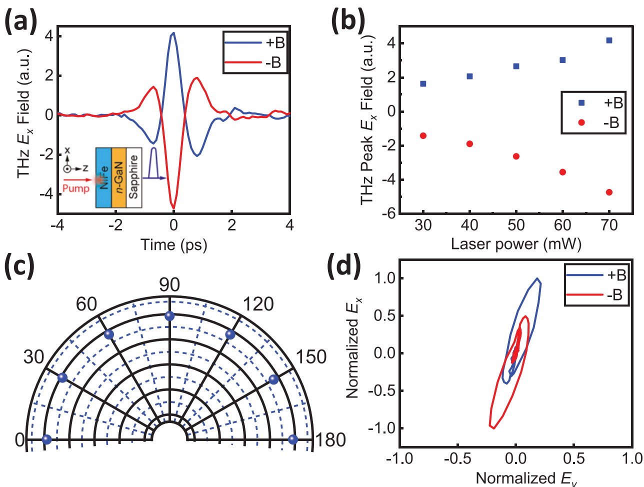

FIG. 2. (a) Typical time trace of the measured THz-electric field from the *n*-GaN ($n = 5 \times 10^{16}$)/NiFe heterostructure under positive ($+B$) and negative ($-B$) magnetic fields, respectively. The emitted THz pulse changes phase with the applied magnetic field. (b) Dependence of the peak-to-peak THz-electric field amplitude on the pump laser power. (c) Normalized peak amplitude of the generated THz-electric field as a function of the rotation of the laser polarization. (d) Parametric plot of THz-electric field amplitudes, which are both polarized along the x-direction, confirming their spintronic nature.

laser. The absence of significant angular dependence is consistent with literature reports of spintronic THz emission.[32] A parametric plot of the THz electric field shows that the polarization of the emitted THz pulse is mainly along the x-direction as a cross product of the NiFe

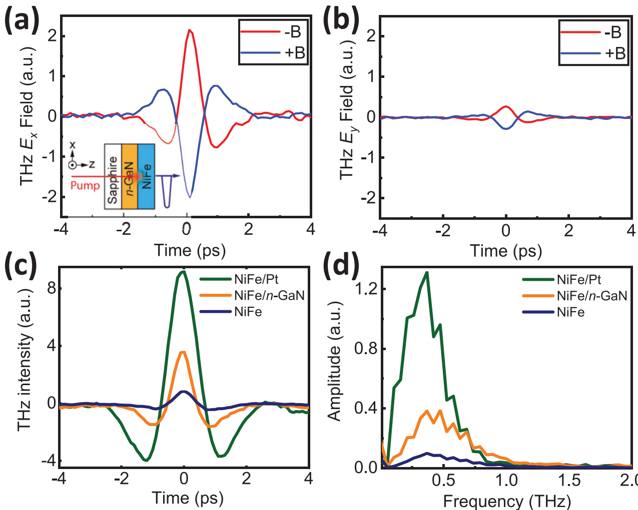

FIG. 3. Time traces of E_x (a) and E_y (b) components of the generated THz-electric field in the same NiFe/n-GaN sample using a back-pump configuration, i.e., ultrafast laser pulse is excited through the sapphire substrate. The position of zero time is chosen arbitrarily. (c) and (d) Comparison of the time- and frequency-domain of the THz-electric field along the x-direction for NiFe(5 nm)/Pt(5 nm), NiFe(5 nm)/*n*-GaN(300 nm), and bare NiFe(5 nm) samples, respectively.

magnetization along the y-direction (M_{+y}) and the spin diffusion direction ($J_{+z}(s)$) along the z-direction (i.e., $E_{-x} \propto J_{+z}(s) \times M_{+y}$).[12]

The E_x and E_y components of the linearly polarized THz emission when excited from the back side of the sample are shown in Figs. 3(a) and 3(b), respectively. In this inverted measurement geometry, the excitation laser pulse is incident first upon the sapphire substrate before transmitting across the *n*-GaN layer (~300 nm-thick) and then ultimately reaching the NiFe layer. The 800 nm laser pump pulse is transparent to both the sapphire substrate and the *n*-GaN film given their wide bandgaps. Thus, the THz emission process is still the same as in the case of normal measurement geometry as shown in Fig. 2. However, while the orientation of the external magnetic field (i.e., magnetization of the NiFe layer along the +y direction) remains the same, the spin current vector, $J_{-z}(s)$ is reversed in the back-pump configuration (i.e., the spin current is still injected from NiFe into the n-GaN but along the -z direction), resulting in an inverted phase of the emitted THz waveform as observed in both E_x and E_y components of Figs. 3(a) and 3(b). This sample orientation dependence experiment unambiguously confirms the spintronic origin of the THz emission from the NiFe/*n*-GaN heterostructure.

Figure 3(c) compares the THz emission from *n*-GaN with that from NiFe/Pt and NiFe-only control samples, with their corresponding Fourier transforms shown in Fig. 3(d). The bandwidth of the THz emission spectra extends up to 1 THz, which is limited in part by the use of the ZnTe crystal in the THz detection setup.[13] It is noted here that the overall THz intensity for NiFe/Pt is roughly two times greater than that in the NiFe/*n*-GaN. While this may be related in part to differences in spin-to-charge conversion efficiencies between the two materials, there are additional contributing factors such as Fabry–Pérot interference that should be taken into account when making comparisons.[13,14,33] The lack of significant THz emission from the NiFe-only control sample rules out the possible THz generation stemming from the non-linear optical or interfacial-related ISHE process in the NiFe layer, which has been reported before in the pure Co films.[32,34] All the control experiments confirm that the origin of the emitted THz radiation is from the ultrafast spin-to-charge conversion occurring in the *n*-GaN layer.

Figure 4(a) shows the dependence of the peak THz emission intensity on the doped carrier concentration in the *n*-GaN layer under 1 mJ/cm^2 (i.e., 70 mW, 3 mm spot size) laser excitation in the normal

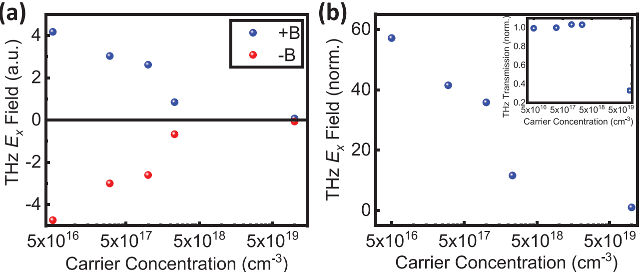

FIG. 4. (a) Peak amplitude of the THz-electric field as a function of carrier concentration in the NiFe/*n*-GaN samples under two magnetic fields. (b) Carrier concentration dependent amplitude of THz radiation normalized by the THz transmission through the device structure. The inset shows the measured THz transmission (0.2–2 THz) as a function of carrier concentration.

Published under license by AIP Publishing

incidence measurement geometry, which represents the main finding of our work. Remarkably, we found that the emitted THz intensity drops logarithmically as the semiconductor layer is doped to successively higher carrier concentrations. It is noteworthy that this decrease cannot be explained by the influence of effective spin mixing conductance formed at the metal/semiconductor interface, which is not subject to the impedance mismatch problem as reported in the Fe/doped-GaAs system under microwave excitations in the GHz range.[35] By reversing the applied magnetic field, the inverted phase of roughly symmetric THz intensity confirms that the generated THz emission is still dominated by the ultrafast spin-to-charge conversion process in the n-GaN film as discussed before.

One possible explanation for this decrease could be a simple reduction in THz transmission through the entire sample structure as a function of carrier concentration. According to the Drude model, the dielectric permittivity of a material is dependent on its free electron density. An increase in carrier density may result in a decrease in the dielectric permittivity of the material in the THz frequency regime and a concomitant increase in the plasma energy. This combined effect may work to suppress the transmission of the THz electric field.[36] To verify this possibility, a normalized plot of the THz transmission (0.2–2 THz) as a function of carrier concentration is presented in Fig. 4(b), with the inset showing peak THz intensity normalized by the transmission for different carrier concentrations. It is shown that the THz transmission is relatively constant across a wide range of carrier concentrations, and even though it decreases by a factor of 3 in the highest concentration sample ($1 \times 10^{20}\,\mathrm{cm}^{-3}$), the THz emission intensity by this point has already decreased by a factor of 60 and, thus, cannot solely account for the observed behavior.

A second possibility that may play a role in the observed carrier concentration dependence of the THz emission intensity is related to the Schottky barrier that forms at the metal/semiconductor interface when the metallic NiFe layer is put in contact with the semiconducting n-GaN layer, given the difference in work functions between the two materials (NiFe = 4.8[37] and GaN = 4.1[38]). This results in the formation of a depletion region at the metal–semiconductor interface, the width of which is inversely proportional to the square root of the doping concentration in the semiconductor. In addition, the resulting electric field at the interface, according to Gauss's law, is linearly proportional to the square root of the doping concentration and will have a fixed electrical polarization. A tuning of this interface electric field as a function of carrier concentration may affect the spin-to-charge conversion efficiency of the Rashba state by shifting the spin-split bands in reciprocal space, similar to what has been observed through gating experiments in Rashba-split 2DEG systems.[39] Since only n-doped GaN was investigated in this study, the polarity of the electric field in the depletion region is fixed and, thus, would be akin to gating with only one voltage polarity. Further experiments in order to elucidate the exact mechanism behind the observed behavior are warranted.

In conclusion, we report the observations of the spintronic THz emission from the NiFe/n-GaN heterostructure as a function of carrier concentration in the semiconductor layer. Not only do we observe THz emission even in a wide bandgap semiconductor, owing to the superdiffusive nature of the operating spin current, but also we found that THz emission intensity decreases exponentially with the increasing n-type carrier concentration. Several possible explanations for the observed behavior related to the Rashba spin-splitting state are offered. This work offers exciting prospects for both the development of semiconductor-based spintronic THz devices and fundamental physics.

AUTHORS' CONTRIBUTIONS

E.V. and M.B. contributed equally to this work.

E.V. and D.S. acknowledge the support from the National Science Foundation, No. ECCS-1933297, and NC State University-Nagoya Research Collaboration Grant. M.B., D.S., and K.G. acknowledge the support from ROI from the UNC system. P.R., R.K., Z.S., and R.C. acknowledge the partial support from the National Science Foundation (Nos. ECCS-1916800, ECCS-1610992, and ECCS-1653383) and the Air Force Office of Scientific Research (AFOSR) (No. FA-95501710225).

DATA AVAILABILITY

The data that support the findings of this study are available from the corresponding authors upon reasonable request.

REFERENCES

[1] M. Tonouchi, Nat. Photonics **1**, 97 (2007).
[2] S. Zhong, Front. Mech. Eng. **14**, 273 (2019).
[3] S. Fan, T. Li, J. Zhou, X. Liu, X. Liu, H. Qi, and Z. Mu, AIP Adv. **7**, 115202 (2017).
[4] A. Redo-Sanchez, N. Laman, B. Schulkin, and T. Tongue, J. Infrared, Millimeter, Terahertz Waves **34**, 500 (2013).
[5] M. Naftaly, N. Vieweg, and A. Deninger, Sensors **19**, 4203 (2019).
[6] J. Federici and L. Moeller, J. Appl. Phys. **107**, 111101 (2010).
[7] T. Kleine-Ostmann and T. Nagatsuma, J. Infrared, Millimeter, Terahertz Waves **32**, 143 (2011).
[8] H. Song and T. Nagatsuma, IEEE Trans. Terahertz Sci. Technol. **1**, 256 (2011).
[9] S. Schlauderer, C. Lange, S. Baierl, T. Ebnet, C. P. Schmid, D. C. Valovcin, A. K. Zvezdin, A. V. Kimel, R. V. Mikhaylovskiy, and R. Huber, Nature **569**, 383 (2019).
[10] J. Walowski and M. Münzenberg, J. Appl. Phys. **120**, 140901 (2016).
[11] T. Kampfrath, A. Sell, G. Klatt, A. Pashkin, S. Mährlein, T. Dekorsy, M. Wolf, M. Fiebig, A. Leitenstorfer, and R. Huber, Nat. Photonics **5**, 31 (2011).
[12] T. Kampfrath, M. Battiato, P. Maldonado, G. Eilers, J. Nötzold, S. Mährlein, V. Zbarsky, F. Freimuth, Y. Mokrousov, S. Blügel, M. Wolf, I. Radu, P. M. Oppeneer, and M. Münzenberg, Nat. Nanotechnol. **8**, 256 (2013).
[13] T. Seifert, S. Jaiswal, U. Martens, J. Hannegan, L. Braun, P. Maldonado, F. Freimuth, A. Kronenberg, J. Henrizi, I. Radu, E. Beaurepaire, Y. Mokrousov, P. M. Oppeneer, M. Jourdan, G. Jakob, D. Turchinovich, L. M. Hayden, M. Wolf, M. Münzenberg, M. Kläui, and T. Kampfrath, Nat. Photonics **10**, 483 (2016).
[14] Y. Wu, M. Elyasi, X. Qiu, M. Chen, Y. Liu, L. Ke, and H. Yang, Adv. Mater. **29**, 1603031 (2017).
[15] D. Yang, J. Liang, C. Zhou, L. Sun, R. Zheng, S. Luo, Y. Wu, and J. Qi, Adv. Opt. Mater. **4**, 1944 (2016).
[16] G. Torosyan, S. Keller, L. Scheuer, R. Beigang, and E. T. Papaioannou, Sci. Rep. **8**, 1311 (2018).
[17] K. Ando, S. Takahashi, J. Ieda, Y. Kajiwara, H. Nakayama, T. Yoshino, K. Harii, Y. Fujikawa, M. Matsuo, S. Maekawa, and E. Saitoh, J. Appl. Phys. **109**, 103913 (2011).
[18] T. Seifert, S. Jaiswal, M. Sajadi, G. Jakob, S. Winnerl, M. Wolf, M. Kläui, and T. Kampfrath, Appl. Phys. Lett. **110**, 252402 (2017).
[19] L. Cheng, X. Wang, W. Yang, J. Chai, M. Yang, M. Chen, Y. Wu, X. Chen, D. Chi, K. E. J. Goh, J. X. Zhu, H. Sun, S. Wang, J. C. W. Song, M. Battiato, H. Yang, and E. E. M. Chia, Nat. Phys. **15**, 347 (2019).
[20] H. Amano, Y. Baines, E. Beam, M. Borga, T. Bouchet, P. R. Chalker, M. Charles, K. J. Chen, N. Chowdhury, R. Chu, C. De Santi, M. M. De Souza, S. Decoutere, L. Di

Published under license by AIP Publishing

Cioccio, B. Eckardt, T. Egawa, P. Fay, J. J. Freedsman, L. Guido, O. Häberlen, G. Haynes, T. Heckel, D. Hemakumara, P. Houston, J. Hu, M. Hua, Q. Huang, A. Huang, S. Jiang, H. Kawai, D. Kinzer, M. Kuball, A. Kumar, K. B. Lee, X. Li, D. Marcon, M. März, R. McCarthy, G. Meneghesso, M. Meneghini, E. Morvan, A. Nakajima, E. M. S. Narayanan, S. Oliver, T. Palacios, D. Piedra, M. Plissonnier, R. Reddy, M. Sun, I. Thayne, A. Torres, N. Trivellin, V. Unni, M. J. Uren, M. Van Hove, D. J. Wallis, J. Wang, J. Xie, S. Yagi, S. Yang, C. Youtsey, R. Yu, E. Zanoni, S. Zeltner, and Y. Zhang, J. Phys. D **51**, 163001 (2018).

[21] J. Y. Tsao, S. Chowdhury, M. A. Hollis, D. Jena, N. M. Johnson, K. A. Jones, R. J. Kaplar, S. Rajan, C. G. Van de Walle, E. Bellotti, C. L. Chua, R. Collazo, M. E. Coltrin, J. A. Cooper, K. R. Evans, S. Graham, T. A. Grotjohn, E. R. Heller, M. Higashiwaki, M. S. Islam, P. W. Juodawlkis, M. A. Khan, A. D. Koehler, J. H. Leach, U. K. Mishra, R. J. Nemanich, R. C. N. Pilawa-Podgurski, J. B. Shealy, Z. Sitar, M. J. Tadjer, A. F. Witulski, M. Wraback, and J. A. Simmons, Adv. Electron. Mater. **4**, 1600501 (2018).

[22] W. Stefanowicz, R. Adhikari, T. Andrearczyk, B. Faina, M. Sawicki, J. A. Majewski, T. Dietl, and A. Bonanni, Phys. Rev. B **89**, 205201 (2014).

[23] J. C. R. Sánchez, L. Vila, G. Desfonds, S. Gambarelli, J. P. Attané, J. M. De Teresa, C. Magén, and A. Fert, Nat. Commun. **4**, 2944 (2013).

[24] F. Kaess, S. Mita, J. Xie, P. Reddy, A. Klump, L. H. Hernandez-Balderrama, S. Washiyama, A. Franke, R. Kirste, A. Hoffmann, R. Collazo, and Z. Sitar, J. Appl. Phys. **120**, 105701 (2016).

[25] G. P. Zhang and W. Hübner, Phys. Rev. Lett. **85**, 3025 (2000).

[26] M. Battiato, K. Carva, and P. M. Oppeneer, Phys. Rev. Lett. **105**, 027203 (2010).

[27] A. Eschenlohr, M. Battiato, P. Maldonado, N. Pontius, T. Kachel, K. Holldack, R. Mitzner, A. Föhlisch, P. M. Oppeneer, and C. Stamm, Nat. Mater. **12**, 332 (2013).

[28] G. M. Choi, B. C. Min, K. J. Lee, and D. G. Cahill, Nat. Commun. **5**, 4334 (2014).

[29] W. Weber, S. D. Ganichev, S. N. Danilov, D. Weiss, W. Prettl, Z. D. Kvon, V. V. Bel'kov, L. E. Golub, H. I. Cho, and J. H. Lee, Appl. Phys. Lett. **87**, 262106 (2005).

[30] J. H. Buß, J. Rudolph, F. Natali, F. Semond, and D. Hägele, Phys. Rev. B **81**, 155216 (2010).

[31] M. Battiato and K. Held, Phys. Rev. Lett. **116**, 196601 (2016).

[32] T. J. Huisman, R. V. Mikhaylovskiy, J. D. Costa, F. Freimuth, E. Paz, J. Ventura, P. P. Freitas, S. Blügel, Y. Mokrousov, T. Rasing, and A. V. Kimel, Nat. Nanotechnol. **11**, 455 (2016).

[33] M. Chen, R. Mishra, Y. Wu, K. Lee, and H. Yang, Adv. Opt. Mater. **6**, 1800430 (2018).

[34] J. Shen, X. Fan, Z. Chen, M. F. DeCamp, H. Zhang, and J. Q. Xiao, Appl. Phys. Lett. **101**, 072401 (2012).

[35] K. Ando, S. Takahashi, J. Ieda, H. Kurebayashi, T. Trypiniotis, C. H. W. Barnes, S. Maekawa, and E. Saitoh, Nat. Mater. **10**, 655 (2011).

[36] T. Kleine-Ostmann, M. Koch, and P. Dawson, Microwave Opt. Technol. Lett. **35**, 343 (2002).

[37] D. Takane, S. Souma, T. Sato, T. Takahashi, K. Segawa, and Y. Ando, Appl. Phys. Lett. **109**, 091601 (2016).

[38] J. I. Pankove and H. Schade, Appl. Phys. Lett. **25**, 53 (1974).

[39] Q. Song, H. Zhang, T. Su, W. Yuan, Y. Chen, W. Xing, J. Shi, J. Sun, and W. Han, Sci. Adv. **3**, e1602312 (2017).

Published under license by AIP Publishing